Emergent Scientist **6**, 3 (2022)
https://doi.org/10.1051/emsci/2022001

Emergent Scientist

Available online at:
https://emergent-scientist.edp-open.org

IPT 2019

RESEARCH ARTICLE OPEN ACCESS

Spatial distribution of air bubbles created by an imping water jet into a free water surface

Alexandre Bense[1,*], Mathieu Lizee[1], Thibault Guillet[2], and Guilhem Gallot[3]

[1] Ecole Polytechnique, Route de Saclay, 91120 Palaiseau, France
[2] LadHyX, UMR 7646 du CNRS, Ecole Polytechnique, Boulevard des Maréchaux, 91120 Palaiseau, France
[3] LOB, UMR 7645 du CNRS, Ecole Polytechnique, Avenue Chasles, 91120 Palaiseau, France

Received: 19 February 2021 / Accepted: 30 September 2021

Abstract. In this paper we study the rise to the surface, radial motion and disappearance of the bubbles created by a water jet pouring into a container, in particular their density at the surface as a function of the impact velocity. We first focus on their emergence radius at the surface which follows a log-normal distribution. Next, we establish experimentally a law relating the bubble velocity to the distance to the jet. We also investigate their disappearance, caused at low density mainly by explosion, and at high density predominantly by coalescence. Finally, we build an accurate model for the density of bubbles.

Keywords: Air Entrainment / plunging Jet / statistical modelling.

1 Introduction

The entrainment of air from a water jet impinging a water surface plays an important role in many hydraulic industrial processes, such as in pipe systems, syphons and hydraulic turbines, or during air cooling of machines, as well as in water chutes or in the vortex found in bathtubs. In physics, plunging water jets into a free water surface are also models for numerous mechanical penetration of one phase into another. Indeed, a jet of water falling onto a free surface with sufficient speed traps air and creates bubbles in the water [2–4]. Pushed up by the buoyant force, these bubbles reach the surface and survive for a few seconds under a thin water film. These "runaway bubbles" acquire a radial motion at the surface, escaping the jet before disappearing. Here, we study the creation, volume expansion and distribution, as well as disappearing of the bubbles created by the water jet. In particular, we present an experimental study and statistical modelling of the bubble spatial distribution on the free water surface.

2 Methods

Assumptions: Water is considered as a homogeneous and incompressible fluid. The main parameters used in the following are shown in Table 1. Therefore, we can neglect the effects of viscosity because the Reynolds number $R_e = \frac{\rho e v_c}{\eta} = 10^4 \gg 1$. We have limited ourselves to the study of cylindrical continuous jets to avoid the angular dependency of the distribution.

2.1 Experimental setup

The setup is described in Figure 1. The experiment requires a free surface and a cylindrical jet. Thus, we poured water into a container of square section 50×50 cm, partially filled with water to a height $h = 30$ cm beforehand. We used a first camera to observe the bubbles underwater through the side of the tank and a second one was placed overhead to observe the free surface. The positions of these two cameras are shown in Figure 1.

Water flowed down to the tank from a hole at the base of a second container placed over the first one at a height H. This second one had a circular cross-section of radius $R_S = 4.5 \pm 0.1$ cm, a height $h_0 = 15.0 \pm 0.1$ cm and a circular hole of radius $R_s = 0.80 \pm 0.02$ cm to pour water.

The first challenge of this study was to record the experimental parameters, such as the impact velocity v, as shown in Figure 1. To do so, we applied the Torricelli Formula and the Bernoulli Theorem with the aforementioned assumptions to get the velocity v as a function of time t:

$$v(t) = \sqrt{2gH + 2gh_0(1 - \frac{t}{\tau})} \text{ with } \tau = \sqrt{\frac{2h_0}{g}}\frac{R_S^2}{r_s^2} \quad (1)$$

* e-mail: alexandre.bense@polytechnique.edu

Table 1. Table with the main parameters. OoM stands for Order of Magnitude.

Quantity	Symbol	Value	Unit
Density	ρ	10^3	kg m^{-3}
Viscosity	η	10^{-3}	Pa s
Surface tension	γ	73 10^{-3}	N m^{-1}
Capillary length	l_c	3.4	mm
Size of the bubbles at the surface (OoM)	ϵ	1	cm
Velocity of impact (OoM)	v_c	1	m s^{-1}

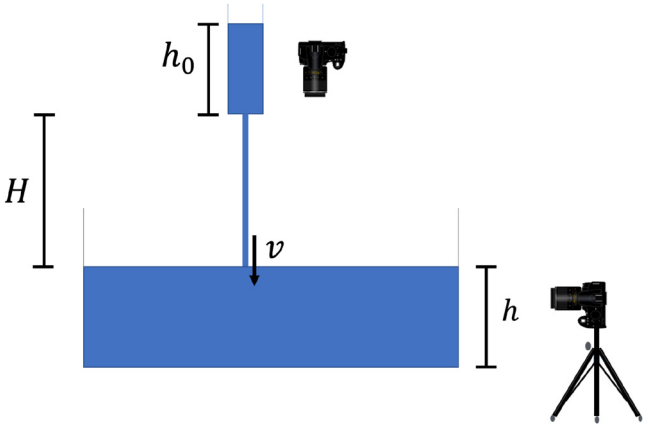

Fig. 1. Experimental setup with the jet of water pouring from a container of depth h_0 at a height H, with an impact velocity v, into a container of depth h.

where $g = 9.81$ m s^{-2} and under our experimental conditions $\tau = 22.3 \pm 1.7$ s. As the average life time of a bubble is 1.6 ± 0.1 s $\approx 0.07\tau$, with a threshold of 10% we can reasonably assume for the following to be in stationary regime.

2.2 Density of bubbles at the surface

To determine the density of bubbles N at the free surface in relation to the distance to the jet, we recorded videos using the top camera, as shown in Figure 2. The density $N(r)$ is defined as the number of bubbles between r and $r + \epsilon$ because ϵ is considered to be the characteristic distance of our phenomenon.

2.3 Tracking the bubbles

To determine the density, we followed the distance to the jet R_a at which the bubbles reach the surface. To do so, we used the side camera from Figure 1 to record the flow of bubbles as shown on Figure 3. We then used the Tracker software 5.0.6 [7] to automatically track the position of the bubbles from the videos recorded by the cameras. Therefore we had access to the trajectory, R_a and to the velocity v_b of every single bubble.

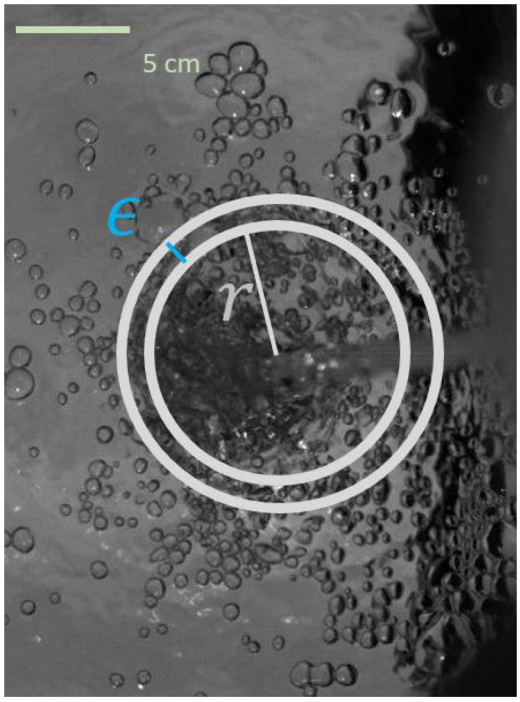

Fig. 2. Experimental picture taken from above, used to measure the density of bubbles at the surface of the container.

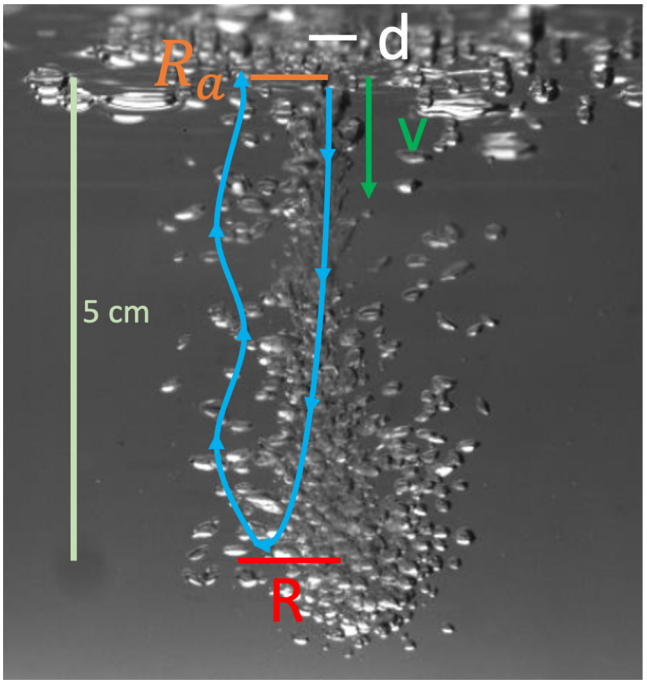

Fig. 3. Example of flow of bubbles created underwater by the jet. R is the largest radius of the flow, v is the impact velocity, d is the diameter of the plunging jet, in blue we have the trajectory of an average bubble with R_a the radius of emergence at the surface.

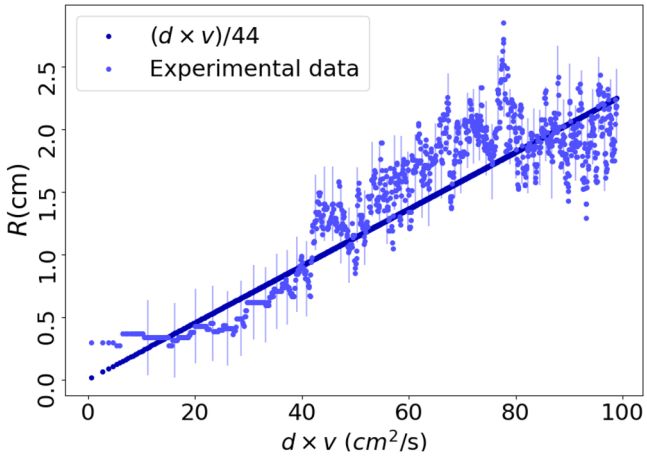

Fig. 4. R as a function of $d \times v$, d is the diameter of the plunging jet, $h = 30$ cm.

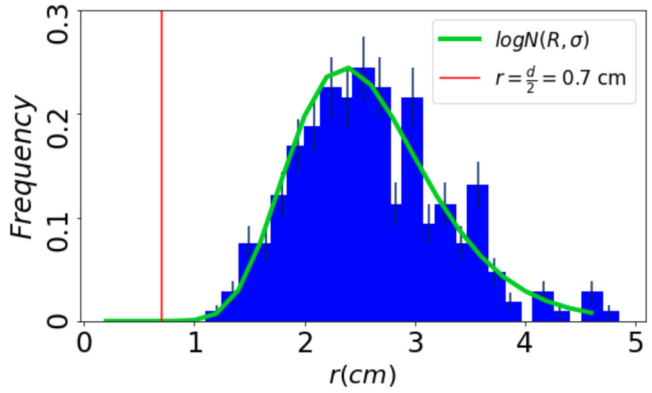

Fig. 5. Histogram of R_a, $\sigma = 6.75 \pm 0.04$ mm, $\mu = R = 26 \pm 3$ mm, $d = 1.4 \pm 0.04$ cm. As described in Figure 3 R_a must be larger than $\frac{d}{2}$ which is represented here in Figure 5 with the vertical red line.

3 Results and discussion

3.1 Rising of the bubbles

The videos clearly established that the bubbles arrive at different radii R_a at the surface, therefore we can consider R_a as a random variable. In this study we especially investigated the expectation μ of the law R_a.

It was observed that most bubbles (≈90%) leave the column of bubbles at the depth at which the radius of the column was the largest as shown in Figure 3, and that they subsequently ascend vertically. Thus we assumed that μ was the largest radius R of the flow, represented in Figure 3. Theoretically, we can obtain R by applying the conservation of the linear momentum, as shown and experimentally verified in [1], which considers that, in a jet, the product of the diameter of the flow d with the velocity v remains constant. With the constant of $0.44\,\mathrm{m\,s^{-1}}$ coming directly from [1], we then theoretically obtain:

$$R = \frac{d \times v}{0.44}. \tag{2}$$

To experimentally verify the relation (2), we measure R for different velocities of impact. The plot of R as a function of $d \times v$ is shown in Figure 4. We observe that equation (2) is in very good agreement with the experimental data. Thus, for each velocity we can make global predictions about R and thus about the expectation μ which will be an important parameter for the law of R_a:

$$\mu = R = \frac{d \times v}{0.44} \tag{3}$$

To determine the law of R_a, we tracked numerically the movement of about 300 bubbles from the videos taken from the side, which allowed us to measure R_a for each bubble and plot its histogram in Figure 5. The acquisition of this tracking lasted 2.00 ± 0.02 s $\approx 0.09\tau$ which does not question the stationarity assumptions. We can notice that the distribution in Figure 5 grows rapidly, reaches a maximum and then decreases more slowly. It can be noted that this distribution is extremely similar to the bubble size distribution in the flow, which can be obtained and studied by acoustic methods [5] or three-dimensional methods called synthetic aperture imaging using multiple cameras and backlight [6]. We can then investigate if the bubble size and R_a are correlated which would explain the similarity between their distributions. To do so, we followed 100 bubbles under water and obtained their diameters. The distribution is in agreement with the articles [5] and [6] with an average diameter of 2.7 ± 0.3 mm which is of the same order of magnitude as the cappillary length l_c. We then performed a Pearson correlation test which proved that R_a and bubble size are decorrelated phenomena (p-value of 0.95 with H_0: no correlation). Therefore, the exact origin of the shape of this distribution is not the size of the bubbles.

For modeling purposes we can then compare the data of R_a with the histograms of the log-normal distribution as shown in Figure 5 and observe that the agreement is excellent. Although the overall shape of the distribution might suggest a normal distribution, the log-normal distribution more accurately describes the heavy tail and the strict positivity of R_a.

If we only consider the accumulation of the bubbles at the surface without disappearance, i.e. for low r, we have:

$$N(r) = \sum_{i=1}^{N_0} P(R_i \leq r)$$

R_i is the observation of R_a for the bubble i and $P(R_i \leq r)$ is the probability that $R_i \leq r$. Having determined the law of R_a, we can now establish a model for the density of the rising bubbles at low r (the model is different at high r and will be developed in the paragraph *Disappearance of the Bubbles* on page 4). As the R_i all follow the same

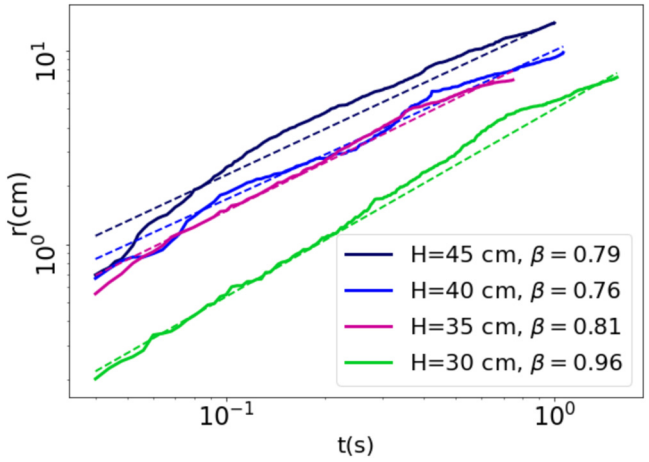

Fig. 6. Different tracking of bubbles in function of time, H is the height through which the jet falls, β is the linear coefficient, $r^2 = 0.97$.

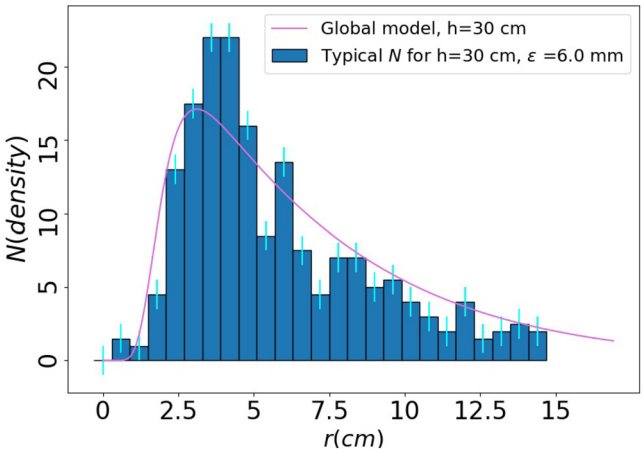

Fig. 7. Example of density of bubbles in function of the distance to the jet compared with the global model from equation (9).

log-normal law, we have with equation 3:

$$N(r) = N_0 P(R_0 \leq r) \text{ and } R_0 \sim \text{Log}\mathcal{N}(\mu = \frac{d \times v}{0.44}, \sigma) \tag{4}$$

3.2 Velocity of bubbles at the surface

The dependence of bubble velocity with time is an important experimental factor, correlated with the bubble density at the surface. Different examples of bubbles tracking are shown in Figure 6. We observe a linear relation between $\log(r)$ and $\log(t)$ with log the natural logarithm, which is confirmed by the coefficient of determination $r^2 = 0.97$. We define β the linear coefficient between $\log(r)$ and $\log(t)$ and we can experimentally obtain the mean of the β: $\overline{\beta} = 0.85 \pm 0.1$ which gives: $r(t) \propto t^{\overline{\beta}}$. This yields the following quantitative relation between the velocity of the bubbles v_b and the distance to the jet r:

$$v_b = \frac{dr}{dt} \propto r^{\frac{\overline{\beta}-1}{\overline{\beta}}} \text{ with } \overline{\beta} = 0.85. \tag{5}$$

The value of $\overline{\beta}$ will be discussed in *Motion of the bubbles* section.

3.3 Maximum density of bubbles at the surface

With the method explained earlier in Methods in the Section *Density of Bubbles at the Surface*, we can obtain the density of bubbles in function of the distance to the jet as shown in Figure 7. We can observe that the density increases for low r, i.e. close to the point of impact of the jet, which is due to the rising of the bubbles and their emergence at the surface. The density then decreases because of the disappearance of the bubbles, described in *Disappearance of the bubbles* section. Thus we observe that every density distribution exhibited a maximum value N_0 as the one shown in Figure 7, which could be easily computed and then used as a reference value for our analytical

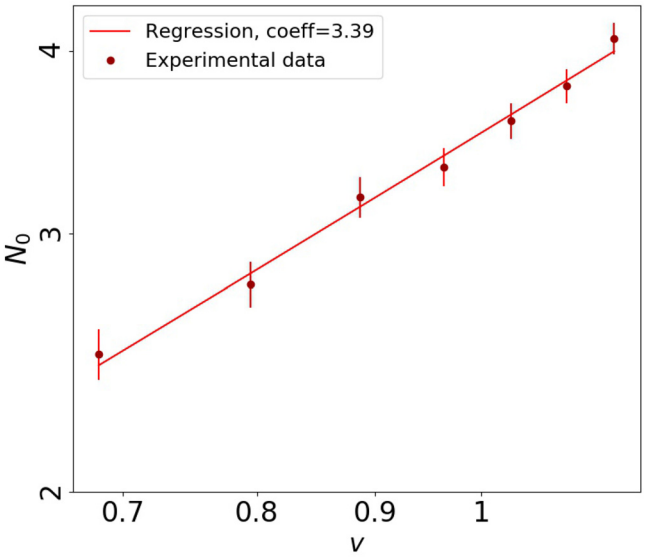

Fig. 8. Values of N_0 in function of the velocity v with a linear regression from which $N_0 \propto v^{3.39}$ and $r^2 = 0.97$.

model of the density. We obtained experimentally the maximum density N_0 for different velocities of impact v, as shown in Figure 8 with the linear regression between $\log(N_0)$ and $\log(v)$. We find that $N_0 \propto v^{3.39}$, which is confirmed by a coefficient of determination $r^2 = 0.97$.

This result can be compared to theoretical results from [3], where it is shown that for laminar flow at low velocity ($v < 4$ m/s), the bubbles are created when the surface tension equals the dynamic pressure in the flow. This equation leads to an air entrainment q_v proportional to v^3. Then, if we assume that all the bubbles have the same volume, N_0 is proportional to the volume flow rate of bubbles. Assuming that the volume flow rate of the bubbles is proportional to the air entrainment rate of the water jet q_v, we obtain for $v < 4\,\text{m/s}$ (indeed we have $1.5 < v < 3\,\text{m/s}$):

$$N_0 \propto q_v \propto v^3 \tag{6}$$

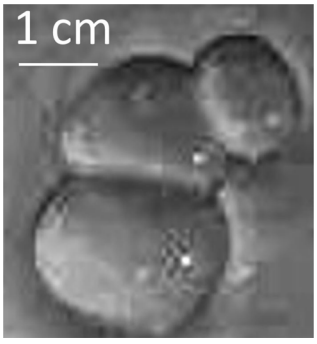

Fig. 9. Coalescence.

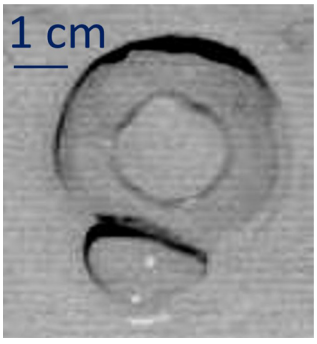

Fig. 10. Explosion.

Consequently, we can now use equation (6) to obtain the reference point for each velocity of our model of the distribution of the bubbles at the free surface, which will be developed in *Global Density Law* section.

3.4 Disappearance of the bubbles

Finally, we need to understand how the bubbles disappear. One bubble indeed has two different destinies: it can coalesce, i.e. merge with another bubble, or explode by itself. These two destinies are represented respectively in Figures 9 and 10.

First, the coalescence is similar to a prey-predator problem. Indeed, the coalescing bubbles absorb their neighbours and are therefore similar to predators. Therefore, the probability that two bubbles coalesce is only the probability that they meet each other, which rises linearly with the density of the bubbles (C.f Appendix A). Thus, the proportion of coalescing bubbles should also rise linearly with the density of the bubbles.

Second, the explosion is due to bubbles disappearing independently of their neighbours (the explosion being due to the drainage of the water film). Consequently, the explosion probability has to be constant with the density of the bubbles.

Thanks to these two considerations, we are able to predict the proportion of bubbles with a stochastic model, cf Appendix A:

$$P_{coalescence} = 1 - e^{-\propto \int_{r=0}^{\infty} \frac{N(r)}{r} \mathrm{dr}} \tag{7}$$

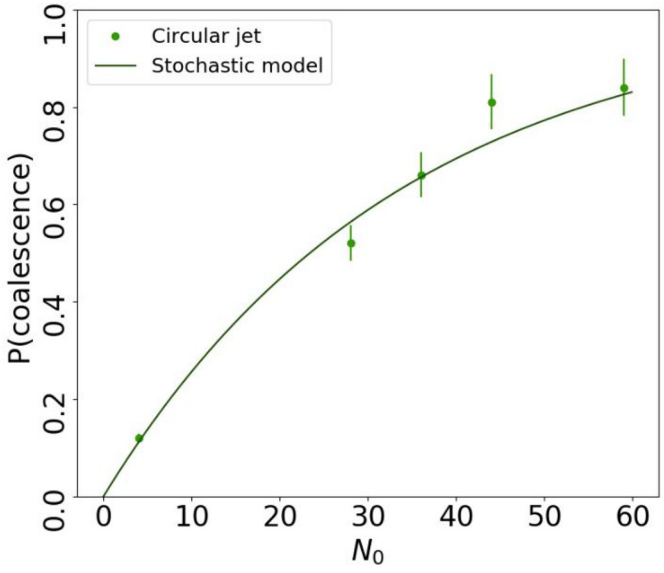

Fig. 11. Experimental proportion of bubbles coalescing as a function of N_0 and theoretical value from the equation (7).

To obtain experimentally the proportion of bubbles we followed the final state of each bubble on images from above such as the one shown in Figure 3. Figure 11 represents the comparison between the experimental proportion of bubbles coalescing as a function of N_0 with the equation (7) (with $N(r)$ verifying the Eq. (4)). The main conclusion of Figure 11 is that coalescence is dominant at high density, while explosion is dominant at low density. This result was expected given equation (7) and helps us understand the phenomenon of disappearance of the bubbles. However, we could refine this result by calculating the proportion of coalescing bubbles for each distance to the jet r, because the result we have first established here is only global and does not depend on r.

Now we can establish a model for high r with the decrease of $N(r)$. We begin by establishing a stochastic model (Appendix B):

$$\frac{dN}{dr} = -kr^{\frac{1-\overline{\beta}}{\overline{\beta}}} N(r). \tag{8}$$

Defining k to be the constant of proportionality, integration of equation (8) gives $\log(N(r)) = C - kr^{\frac{1}{\overline{\beta}}}$. With the plot of $\log(N(r))$ against $r^{\frac{1}{\overline{\beta}}}$ in Figure 12, we can confirm equation (8) after a linear regression ($r^2 = 0.97$) and we find k to be 24.02 ± 0.05 m$^{-\frac{1}{\overline{\beta}}}$.

3.5 Global density law

At this point we have understood the different predominant phenomena at low r (rising of the bubbles) and high r (disappearance of the bubbles) and their behaviour with the impact velocity. Consequently we can build an analytical global model of the density.

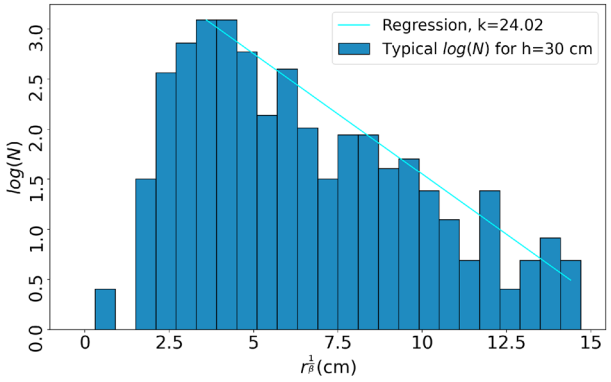

Fig. 12. $\log(N(r))$ in function of $r^{\frac{1}{\beta}}$ with linear regression at high r: $r^2 = 0.97$.

We can merge (4) and (8) to obtain:

$$\frac{dN}{dr} = -kr^{\frac{1-\beta}{\beta}} N(r) + \frac{N_0}{\sigma r\sqrt{2\pi}} e^{(\frac{ln(r)-R}{\sigma\sqrt{2}})^2} \tag{9}$$

This can be solved numerically and the result is represented in Figure 7. We observe that this model is in quite good agreement with the experimental data. Consequently, we have successfully established an analytical model of the density of bubbles, by merging the theory of rising with the theory of disappearance of the bubbles.

However, we can notice in Figure 7, that the maximum of the model does not correspond exactly to the experimental maximum. This seems to come from the fact that we consider the same rate of disappearance for different distances to the jet r. Indeed we found k (defined in Eq. (8)) only at high r, therefore we could refine the model by studying k as a function of r.

4 Dead end

In this part, we will present some experiments that have failed and try to understand why.

4.1 Setup with an overflow

In order to keep v_0 constant, water could be constantly pumped into the second container including an overflow valve to set the height h_0. However, the injection of water strongly perturbs the initial velocity v_0. To avoid this, we had to keep a container emptying without a return system.

4.2 Motion of the bubbles

We hypothesised the motion of the bubbles to be a consequence of impacts between ascending bubbles and bubbles at the surface. In this section, we discuss our previous hypotheses of the origin of the motion of the bubbles and the evidences that refute them.

First, we believed that the motion of the bubbles was caused by a water flow created by the jet of water. We hence placed pepper grains in the water to observe for the motion of the pepper in the water through the camera viewing the side of the tank. However, no motion was observed and we could conclude that the flow of water under the surface was negligible.

We next injected blue ink in the water and we observed that the ink moved only at the surface. Consequently we made our second hypothesis: there was only a thin film of water flow at the surface causing the motion of the bubbles. However, at low water volume flow rate, there were only some bubbles and they did not escape the jet. Furthermore, the conservation of the volume flow rate gave $\beta = 0.5$, while experimentally we had $\beta = 0.85$. Thus, the second hypothesis was also rejected.

Our third hypothesis was that the surface waves were transmitting kinetic energy to the bubbles at the surface. So we put pepper grains only at the surface and not underwater, but the grains did not move until they were hit by a bubble. Furthermore, the surface waves' velocity was constant for a constant depth, which gave $\beta = 1$. Thus this assumption was also false.

Finally at low water volume flow rate, there were only few bubbles, thus there were no impacts between them and they did not escape the jet. At a higher volume flow rate, we observed impacts between the bubbles and, simultaneously, motion of the bubbles at the surface. This led us to hypothesise that the motion is caused by the impacts between bubbles.

5 Conclusion

In this paper we studied the rise to the surface, radial motion and disappearance of the "runaway bubbles" created by a jet pouring into a container, in order to establish their density at the surface as a function of the impact velocity. We first focused on their radius of birth at the surface which follows a log-normal distribution. Next, we studied their motion and we established experimentally the power law (5) relating the bubble velocity to the distance to the jet. We also investigated their disappearance, caused at low density mainly by explosion, and at high density predominantly by coalescence. Finally, we were able to build a global model for the density of bubbles, which fitted conveniently to the experimental data.

Appendix A: Stochastic model for the proportion of bubbles coalescing

The proportion of bubbles coalescing will be here considered as a probability named $P_{coalescence}$.

We use the following notation:
$A_r :=$ [The bubble has merged in r].
$E_r :=$ [The bubble has exploded in r].
$M_r :=$ [The bubble meets an other bubble between r and $r + dr$].
$\frac{N(r)dr}{\epsilon}$ is the number of bubbles between r and r+dr.
$S_r := 2\pi r dr$ is the area between r and $r + dr$.
$S_a := \epsilon dr$ is the scanned area by one bubble in r.
$P(r) := P(A_r)$.

If we assume that the bubbles do not influence the explosion of their neighbors we can consider that the explosion does not depend on r: $P(E_r) = p_e$.

The exponent c refers to the opposite event: for example A_r^c is the opposite event of A_r.

$$\begin{aligned} P(A_{r+dr}|A_r^c) &= P(A_{r+dr}|A_r^c, E_r)P(E_r) \\ &\quad + P(A_{r+dr}|A_r^c, E_r^c)P(E_r^c) \\ &= 0 + (1-p_e)P(M_r) \\ &= (1-p_e)\frac{N(r)dr}{\epsilon}\frac{S_a}{S_r} \\ &= (1-p_e)\frac{N(r)dr}{\epsilon}\frac{\epsilon dr}{2\pi r dr} \\ &= (1-p_e)\frac{N(r)dr}{2\pi r} \end{aligned}$$

$$\begin{aligned} P(A_{r+dr}) &= P(A_{r+dr}|A_r)P(A_r) + P(A_{r+dr}|A_r^c)P(A_r^c) \\ &= p(r) + \frac{(1-p(r))(1-p_e)N(r)dr}{2\pi r} \end{aligned}$$

because $P(A_{r+dr}|A_r) = 1$ and $P(A_r^c) = 1 - P(r)$.

By integration we have:

$$P_{coalescence} = 1 - e^{-\propto \int_{r=0}^{\infty} \frac{N(r)}{r} dr} \tag{A.1}$$

Appendix B: Stochastic model for the disappearance

We are following a set of bubbles according to time. We use the following notation:

$D(\tau) :=$ [bubbles disappearing in r between $t, t+\tau$].

If the set of bubbles is in r at time t we can assume that $\frac{D(dt)}{dt} \propto N(r)$.

Thus:

$$\begin{aligned} \frac{dN}{dr} &\approx \frac{N(r+\epsilon) - N(r)}{\epsilon} \\ &\approx \frac{D(\frac{\epsilon}{v_b(r)})}{\epsilon} \\ &\propto \frac{D(dt)}{v_b(r)dt} \\ &\propto \frac{1}{v_b(r)} N(r) \end{aligned}$$

With equation (5), we obtain:

$$\frac{dN}{dr} \propto r^{\frac{\overline{\beta}-1}{\overline{\beta}}} N(r)$$

References

1. C. Clanet, J.C. Lasheras, Depth of penetration of bubbles entrained by a plunging water jet, Phys. Fluids **9**, 1864–1866 (1997)
2. A.K. Bin, Minimum air entrainment velocity of vertical plunging liquid jets, Chem. Eng. Sci. **43**, 379–389 (1988)
3. K.J. Sene, Air entrainment by plunging jets, Chem. Eng. Sci. **43**, 2615–2623 (1988)
4. É. Lorenceau, D. Quéré, J.Eggers, Air entrainment by a viscous jet plunging into a bath, Phys. Rev. Lett. **93**, 254501 (2004)
5. H. Chanson, R. Manasseh, Air entrainment processes in a circular plunging jet: Void-fraction and acoustic measurements, J. Fluids Eng. **125**, 910–921 (2003)
6. J. Belden, S. Ravela, T.T. Truscott, A.H. Techet, Three-dimensional bubble field resolution using synthetic aperture imaging: application to a plunging jet, Exp. Fluids **53**, 839–861 (2012)
7. D. Brown, Software: Tracker. Version: 5.0.6. Release date: June 2008. Available on: https://getpczone.com/software/tracker-5-0-6-download-64-bit

Cite this article as: Alexandre Bense, Mathieu Lizee, Thibault Guillet, Guilhem Gallot. Spatial distribution of air bubbles created by an imping water jet into a free water surface, Emergent Scientist **6**, 3 (2022)